INTERNATIONAL JOURNAL FOR NUMERICAL METHODS IN FLUIDS, VOL. 25, 779–802 (1997)

CALCULATION OF VERTICAL VELOCITY IN THREE-DIMENSIONAL, SHALLOW WATER EQUATION, FINITE ELEMENT MODELS

J. C. MUCCINO,[1]* W. G. GRAY[1] AND M. G. G. FOREMAN[2]

[1] *Department of Civil Engineering and Geological Sciences, University of Notre Dame, Notre Dame, IN 46556, U.S.A.*
[2] *Institute of Ocean Sciences, Sidney, British Columbia, V8L 4B2, Canada*

SUMMARY

Computation of vertical velocity within the confines of a three-dimensional, finite element model is a difficult but important task. This paper examines four approaches to the solution of the overdetermined system of equations arising when the first-order continuity equation is solved in conjunction with two boundary conditions. The traditional (TRAD) method neglects one boundary condition, solving the continuity equation with the remaining boundary condition. The vertical derivative of continuity (VDC) method involves solution of the second-order equation obtained by differentiation of the continuity equation with respect to the vertical co-ordinate. The least squares (LS) method minimizes the residuals of the continuity equation (in discrete form) and the two boundary conditions. The adjoint (ADJ) method minimizes the residuals of the continuity equation (in continuous form) and the two boundary conditions.

Two domains are considered: a quarter-annular harbour and the southwest coast of Vancouver Island. Results indicate that the highest-quality solution is obtained with both LS and ADJ. Furthermore, ADJ requires less CPU and memory than LS. Therefore the optimal method for computation of vertical velocity in a three-dimensional finite element model is the adjoint (ADJ) method. © 1997 John Wiley & Sons, Ltd.

Int. J. Numer. Meth. Fluids, **25**: 779–802 (1997).

No. of Figures: 14. No. of Tables: 0. No. of References: 23.

KEY WORDS: finite element method; vertical velocity; three-dimensional; Vancouver Island

1. INTRODUCTION

Finite element models of the three-dimensional shallow water equations are commonly used to gain insight into the behaviour of large bodies of water subject to tides and atmospheric stresses. Calculation of vertical velocity within these models is difficult because the vertical speed is often three or four orders of magnitude less than the horizontal speed at the same point. However, in some cases the vertical transport is substantial enough to warrant careful consideration because the horizontal length scales are usually several orders of magnitude larger than the vertical length scales.

* Correspondence to: J. C. Muccino, Department of Civil Engineering and Geological Sciences, University of Notre Dame, Notre Dame, IN 46556, U.S.A.

Contract grant sponsor: National Science Foundation; Contract grant number: R34111-77600094.

CCC 0271–2091/97/070779–24 $17.50

Received 2 July 1996
Revised 16 December 1996

In such cases, accurate prediction of the vertical component of the current is critical to the understanding and management of major fish and zooplankton stocks, as upwelling is believed to be responsible for bringing nutrients towards the surface from deeper regions.

The standard approach to solving the three-dimensional shallow water equations with the finite element method consists of three sequential stages.[1–3] The first stage is the computation of the free-surface elevation with a wave equation that is uncoupled from the velocity for a linear system. Next the horizontal momentum equations are solved to yield the horizontal velocity field, which is a function of the vertical co-ordinate. The final stage involves calculation of the vertical velocity field with the three-dimensional continuity equation.

This paper is concerned solely with the final stage, the vertical velocity calculation. The vertical velocity calculation procedures described here do not depend upon the method used to obtain the elevation and horizontal velocity fields and thus can be implemented in any model that provides those fields.

The vertical velocity computation is addressed as follows. The model used to obtain the elevation and horizontal velocity fields is described in Section 2. Four numerical methods of vertical velocity calculation are described in Section 3. Section 4 describes an application of these four methods to a tidally forced quarter-annular harbour problem, compares the numerical solutions with the analytic solution and compares the mass conservation properties of the numerical approaches. Section 5 presents the results obtained with the four numerical vertical velocity methods applied to the southwester coast of Vancouver Island as well as a conservation of mass analysis.

2. THREE-DIMENSIONAL MODEL FRAMEWORK

The model used to compute the elevation and horizontal velocity fields is a three-dimensional diagnostic model for continental shelf circulation, known as FUNDY5, developed by Lynch *et al.*[4] and Naimie and Lynch.[5] This section will provide a brief overview of the model derivation. The interested reader should refer to these papers for further details.

2.1. Governing equations

FUNDY5 is a finite element model that solves the linearized shallow water equations with conventional hydrostatic and Boussinesq assumptions for periodic motions. The continuity equation is

$$\partial w/\partial z + \nabla \cdot \mathbf{V} = 0, \tag{1}$$

where $w(x, y, z)$ is the vertical velocity, $\mathbf{V}(x, y, z)$ is the horizontal velocity, with components u and v, ∇ is the horizontal del operator, (x, y) are the horizontal co-ordinates and z is the vertical co-ordinate, positive upwards with $z = 0$ at the surface. The linearized vertical average of (1) is

$$\partial \eta/\partial t + \nabla \cdot (h\bar{\mathbf{V}}) = 0, \tag{2}$$

where $\bar{\mathbf{V}}(x, y)$ is the vertical average of $\mathbf{V}(x, y, z)$, $\eta(x, y)$ is the free surface elevation above the reference level, $h(x, y)$ is the bathymetric depth measured from the reference level and t is time.

The three-dimensional linearized horizontal momentum equation is

$$\frac{\partial \mathbf{V}}{\partial t} + \mathbf{f} \times \mathbf{V} - \frac{\partial}{\partial z}\left(N \frac{\partial \mathbf{V}}{\partial z}\right) = \mathbf{G}, \tag{3}$$

where $\mathbf{f} = f\hat{\mathbf{z}}$ is the vector Coriolis parameter, $\hat{\mathbf{z}}$ is the unit vector in the vertical direction, $N(x, y, z)$ is the vertical eddy viscosity, $\mathbf{G} = -g\nabla\eta$ is the barotropic pressure gradient and g is gravity. Boundary conditions on stress are imposed at the free surface and at the bottom:

$$\left[N\frac{\partial \mathbf{V}}{\partial z} = h\boldsymbol{\Psi}\right]_{z=0}, \tag{4}$$

$$\left[N\frac{\partial \mathbf{V}}{\partial z} = k\mathbf{V}\right]_{z=-h}, \tag{5}$$

where $h\boldsymbol{\Psi}(x, y)$ is the atmospheric forcing due to lateral stress and k is the linear bottom stress coefficient. The vertical average of (3), after implementation of boundary conditions (4) and (5), is

$$\frac{\partial \bar{\mathbf{V}}}{\partial t} + \mathbf{f} \times \bar{\mathbf{V}} + \frac{k}{h}\mathbf{V}\bigg|_{-h} = \mathbf{G} + \boldsymbol{\Psi}. \tag{6}$$

The governing equations will be considered in their periodic form such that all time-dependent variables have time variation of the form

$$q(x, y, z, t) = Q(x, y, z)\mathrm{e}^{\mathrm{i}\omega t},$$

where Q is the complex amplitude, ω is the radian frequency and 'i' is the imaginary unit, $\sqrt{(-1)}$. The periodic form of the depth-averaged continuity equation is

$$\mathrm{i}\omega\eta + \nabla \cdot (h\bar{\mathbf{V}}) = 0, \tag{7}$$

and the periodic forms of the three-dimensional momentum equation and the depth-averaged momentum equation are respectively

$$\mathrm{i}\omega\mathbf{V} + \mathbf{f} \times \mathbf{V} - \frac{\partial}{\partial z}\left(N\frac{\partial \mathbf{V}}{\partial z}\right) = \mathbf{G}, \tag{8}$$

$$\mathrm{i}\omega\bar{\mathbf{V}} + \mathbf{f} \times \bar{\mathbf{V}} + \frac{k}{h}\mathbf{V}\bigg|_{-h} = \mathbf{G} + \boldsymbol{\Psi}. \tag{9}$$

Boundary conditions in the horizontal plane are implemented in order to close the boundary value problem. Three types of boundary conditions are allowed: specified elevation, specified normal velocity and geostrophically balanced transport. The response sought is the surface elevation field and the three-dimensional velocity field.

2.2. *Expression of bottom stress as a function of vertically averaged velocity*

The momentum equation (3) is coupled in the horizontal velocity components through the Coriolis term. Introduction of surrogate variables

$$\upsilon^+ = \frac{u + \mathrm{i}v}{2}, \qquad \upsilon^- = \frac{u - \mathrm{i}v}{2}, \tag{10}$$

$$u = \upsilon^+ + \upsilon^-, \qquad \mathrm{i}v = \upsilon^+ - \upsilon^- \tag{11}$$

removes the Coriolis coupling from the momentum equation (3), i.e.

$$\mathrm{i}(\omega \pm f)\upsilon^\pm - \frac{\partial}{\partial z}\left(N\frac{\partial}{\partial z}\upsilon^\pm\right) = G^\pm, \tag{12}$$

and the boundary conditions (4) and (5) become

$$\left[N\frac{\partial v^{\pm}}{\partial z} = h\psi^{\pm}\right]_{z=0}, \tag{13}$$

$$\left[N\frac{\partial v^{\pm}}{\partial z} = kv^{\pm}\right]_{z=-h}, \tag{14}$$

where the forcing terms are defined as

$$G^{\pm} = \frac{G_x \pm \mathrm{i}G_y}{2}, \qquad \psi^{\pm} = \frac{\psi_x \pm \mathrm{i}\psi_y}{2}. \tag{15}$$

Because the momentum equation (12), boundary conditions (13) and (14) and the forcing are linear, consideration of each forcing phenomenon individually reduces (12) to the superposition of two, simple, one-dimensional diffusion problems. The diffusion problems are solved at every node of the horizontal grid with the Galerkin method using linear finite elements. The first diffusion problem is forced with a unit barotropic gradient alone ($G^{\pm} = 1, \psi^{\pm} = 0$) and yields a solution $P_1^{\pm}$; the second diffusion problem is forced with unit atmospheric stress alone ($G^{\pm} = 0, \psi^{\pm} = 1$) and yields a solution $P_2^{\pm}$. Superposition of the two solutions ($P_1^{\pm}, P_2^{\pm}$) yields the solution to (12):

$$v^{\pm} = G^{\pm}P_1^{\pm}(z) + \psi^{\pm}P_2^{\pm}(z). \tag{16}$$

The vertical average of (16) is

$$\bar{v}^{\pm} = G^{\pm}\bar{P}_1^{\pm} + \psi^{\pm}\bar{P}_2^{\pm}. \tag{17}$$

The barotropic pressure gradient $G^{\pm}$ may be eliminated from (16) by (17):

$$kv^{\pm}(-h) = \tau^{\pm}h\bar{v}^{\pm} - \alpha^{\pm}h\psi^{\pm}, \tag{18}$$

where $\tau^{\pm} = kP_1^{\pm}(-h)/(h\bar{P}_1^{\pm})$ and $\alpha^{\pm} = \tau^{\pm}\bar{P}_2^{\pm} - kP_2^{\pm}(-h)/h$. The bottom stress component is obtained in the original (x, y) co-ordinate system according to (10) and (11):

$$k\mathbf{V}(-h) = h\bar{\mathbf{V}}\left(\frac{\tau^{+} + \tau^{-}}{2}\right) - \mathrm{i}h\left(\frac{\tau^{+} - \tau^{-}}{2}\right)\hat{\mathbf{z}} \times \bar{\mathbf{V}} - h\boldsymbol{\Psi}\left(\frac{\alpha^{+} + \alpha^{-}}{2}\right) + \mathrm{i}h\left(\frac{\alpha^{+} - \alpha^{-}}{2}\right)\hat{\mathbf{z}} \times \boldsymbol{\Psi}. \tag{19}$$

Thus bottom stress is now expressed as a function of vertically averaged velocity rather than local velocity.

2.3. Derivation of wave equation

Expression (19) for bottom stress as a function of vertically averaged velocity can be used in (6) to eliminate reference to bottom velocity:

$$(\mathrm{i}\omega + \tau')\bar{\mathbf{V}} + \mathbf{f}' \times \bar{\mathbf{V}} = \mathbf{G} + \boldsymbol{\Psi}', \tag{20}$$

where all vertical details is represented by the primed quantities $\mathbf{f}', \tau'$ and $\boldsymbol{\Psi}'$ given by

$$\mathbf{f}' = \mathbf{f} - \mathrm{i}\tau'\hat{\mathbf{z}}, \qquad \tau' = \frac{\tau^{+} - \tau^{-}}{2},$$

$$\boldsymbol{\Psi}' = \boldsymbol{\Psi}\left[1 + \left(\frac{\alpha^{+} + \alpha^{-}}{2}\right)\right] - \mathrm{i}\left(\frac{\alpha^{+} - \alpha^{-}}{2}\right)\hat{\mathbf{z}} \times \boldsymbol{\Psi}.$$

After some manipulation of (20), $\bar{\mathbf{V}}$ can be written explicitly as

$$\bar{\mathbf{V}} = \frac{(\mathrm{i}\omega + \tau')(\mathbf{G} + \boldsymbol{\Psi}') - \mathbf{f}' \times (\mathbf{G} + \boldsymbol{\Psi}')}{(\mathrm{i}\omega + \tau')^2 + f'^2}. \tag{21}$$

Substitution of (21) into the vertically averaged continuity equation (2) yields the wave equation

$$\mathrm{i}\omega\eta + \nabla \cdot \left(\frac{(\mathrm{i}\omega + \tau')h(\mathbf{G} + \boldsymbol{\Psi}') - \mathbf{f}' \times h(\mathbf{G} + \boldsymbol{\Psi}')}{(\mathrm{i}\omega + \tau')^2 + f'^2} \right) = 0. \tag{22}$$

Incorporation of $\mathbf{G} = -g\nabla\eta$ and rearrangement of terms such that known quantities are on the right and unknown quantities are on the left yields an equation with η as the only dependent variable:

$$\mathrm{i}\omega\eta - \nabla \cdot \left(\frac{(\mathrm{i}\omega + \tau')gh\nabla\eta - \mathbf{f}' \times gh\nabla\eta}{(\mathrm{i}\omega + \tau')^2 + f'^2} \right) = -\nabla \cdot \left(\frac{(\mathrm{i}\omega + \tau')h\boldsymbol{\Psi}' - \mathbf{f}' \times h\boldsymbol{\Psi}'}{(\mathrm{i}\omega + \tau')^2 + f'^2} \right). \tag{23}$$

2.4. Surface elevation

The surface elevation is computed according to the wave equation (23) with the Galerkin method in a horizontal grid of triangular elements. The weighted residual statement for (23), after implementation of the Gauss theorem, is

$$\begin{aligned} &\langle \mathrm{i}\omega\eta, \varphi_i \rangle + \left\langle \left(\frac{(\mathrm{i}\omega + \tau')gh\nabla\eta - \mathbf{f}' \times gh\nabla\eta}{(\mathrm{i}\omega + \tau')^2 + f'^2} \right), \nabla\varphi_i \right\rangle \\ &\quad = -\int_\Gamma \varphi_i h\bar{\mathbf{V}} \cdot \hat{\mathbf{n}} \ \mathrm{d}\Gamma + \left\langle \left(\frac{(\mathrm{i}\omega + \tau')h\boldsymbol{\Psi}' - \mathbf{f}' \times h\boldsymbol{\Psi}'}{(\mathrm{i}\omega + \tau')^2 + f'^2} \right), \nabla\varphi_i \right\rangle, \end{aligned} \tag{24}$$

where $\langle a, b \rangle$ denotes the inner product of a and b, φ_i are weighting functions, Γ is the boundary of the domain Ω and $\hat{\mathbf{n}}$ is the outward unit vector to Γ. The elevation η is approximated as

$$\eta(x, y) = \sum_{j=1}^{3} \eta_j \varphi_j(x, y), \tag{25}$$

where η_j are unknown nodal coefficients and $\varphi_j(x, y)$ are linear triangular basis functions. Substitution of (25) into (24) yields

$$[\mathbf{A}]\{\boldsymbol{\eta}\} = \{\mathbf{B}\} - \{\mathbf{F}\}, \tag{26}$$

where

$$\begin{aligned} A_{ij} &= \langle \mathrm{i}\omega\varphi_j, \varphi_i \rangle + \left\langle \left(\frac{(\mathrm{i}\omega + \tau')gh\nabla\varphi_j - \mathbf{f}' \times gh\nabla\varphi_j}{(\mathrm{i}\omega + \tau')^2 + f'^2} \right), \nabla\varphi_i \right\rangle, \\ B_i &= \left\langle \left(\frac{(\mathrm{i}\omega + \tau')h\boldsymbol{\Psi}' - \mathbf{f}' \times h\boldsymbol{\Psi}'}{(\mathrm{i}\omega + \tau')^2 + f'^2} \right), \nabla\varphi_i \right\rangle, \\ F_i &= \int_\Gamma h\bar{\mathbf{V}} \cdot \hat{\mathbf{n}}\varphi_i \ \mathrm{d}\Gamma. \end{aligned}$$

The domain is discretized in the horizontal by linear triangles. All inner products are evaluated numerically by nodal quadrature.

2.5. Horizontal velocity profiles

Once the surface elevation is known, $\mathbf{G} = -g\nabla\eta$ may be computed. The vertical structure of the horizontal velocity is embedded in the solutions $(P_1^{\pm}, P_2^{\pm})$ and the components of the vertical profiles of the horizontal velocity can be recovered from expression (16) for $v^{\pm}$ according to (11) and (15):

$$\mathbf{V}(z) = \mathbf{G}\left(\frac{P_1^+ + P_1^-}{2}\right) - \mathrm{i}\left(\frac{P_1^+ - P_1^-}{2}\right)\hat{\mathbf{z}} \times \mathbf{G} + \boldsymbol{\Psi}\left(\frac{P_2^+ + P_2^-}{2}\right) - \mathrm{i}\left(\frac{P_2^+ - P_2^-}{2}\right)\hat{\mathbf{z}} \times \boldsymbol{\Psi}. \tag{27}$$

2.6. Vertical velocity profiles

Although the vertical velocity calculation procedures do not depend on the method used to obtain the horizontal velocity field, they do depend on the quality of that method. Any errors in calculation of horizontal velocities will be reflected in the subsequent calculation of vertical velocities; the vertical velocities can be considered to be collectors of error from all previous calculations. As a result, converged elevation and horizontal velocity fields are prerequisites to computations of accurate vertical velocity fields.

A three-dimensional grid is generated by projecting the nodes of the horizontal grid to the bottom of the domain in vertical lines and discretizing each line into a constant number of vertical elements. The resulting three-dimensional grid comprises prismatic elements with vertical, quadrilateral sides and triangular top and bottom faces that are, in general, not parallel to each other. A one-dimensional system is therefore obtained for each node in the horizontal grid and each one-dimensional system is uncoupled from all other one-dimensional systems. A schematic diagram of the vertical discretization is shown in Figure 1. In this work the vertical node spacing for each vertical line is constant. However, since the length of each vertical line is equal to the bathymetric depth at its horizontal location, the length of elements may differ from one vertical line to another.

3. FOUR METHODS OF VERTICAL VELOCITY CALCULATION

The three-dimensional continuity equation as given by

$$\partial w/\partial z = -\nabla \cdot \mathbf{V} \tag{28}$$

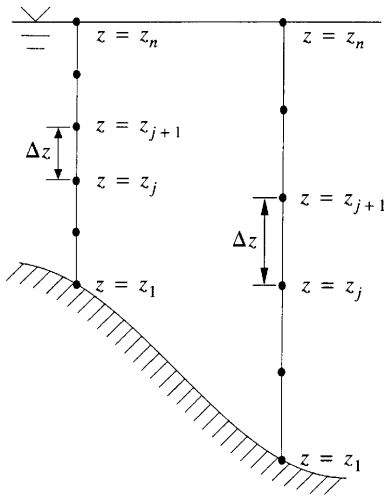

Figure 1. Detail of vertical discretization

is used to compute the vertical velocity w. Since $\nabla \cdot \mathbf{V}$ may be calculated from (27), the continuity equation is an ordinary, first-order differential equation that can satisfy only one boundary condition. In general an estimate of vertical velocity is available at the bottom and the free surface respectively:

$$\left[w = u\frac{\partial h}{\partial x} + v\frac{\partial h}{\partial y}\right]_{z=-h}, \tag{29}$$

$$[w = i\omega\eta]_{z=0}. \tag{30}$$

Either (29) or (30) can serve as the boundary condition, but imposition of both (29) and (30) when solving (28) overdetermines the system. No unique solution exists for an overdetermined system of equations. Four approaches to the solution of this overdetermined system of equations will now be described: the *traditional* method, the *vertical derivative of continuity* method, the *least squares* method and the *adjoint* method.

3.1. Traditional (TRAD) method

Traditionally, the overdetermined continuity system has been solved by simply not enforcing one of the bottom or surface boundary conditions and using the neglected condition as a measure of error accumulated over the water column.[2] In this way the overdetermined system is reduced to a determined one. Unfortunately, because the neglected boundary condition contains valuable information, unsatisfactory accumulation of error over the water column results, with the greatest error occurring at the location where the condition is neglected. In addition, if the enforced condition has any error, that error will be reflected throughout the water column as an additive constant. This approach will henceforth be referred to as 'TRAD'.

3.2. Vertical derivatives of continuity equation (VDC) method

As suggested by Lynch and Werner,[2] an alternative method of vertical velocity calculation involves solution of the second-order equation that results after differentiating (28) with respect to z:

$$\frac{\partial^2 w}{\partial z^2} = -\frac{\partial}{\partial z}(\nabla \cdot \mathbf{V}). \tag{31}$$

Because (31) is a second-order differential equation, both boundary conditions (29) and (30) may be enforced when (31) is solved by the Galerkin finite element method. However, the restriction of the original continuity equation is compromised in favour of the additional boundary condition. The resulting mass conservation properties are studied in Sections 4 and 5. This approach, involving the vertical derivative of the continuity equation, will henceforth be referred to as 'VDC'.

3.3. Least squares method

The first new procedure for calculation of vertical velocity developed in this work involves solution of the continuity equation in its original form and imposition of both boundary conditions. Although the overdetermined system of equations cannot be solved uniquely, the Eulerian norm of the residual may be minimized according to the theory of least squares.[6] By allowing non-zero residuals for the boundary conditions and the original conservation of mass equation, the least squares approach resembles the traditional method, since the original continuity equation is solved. However, it also resembles VDC in that both boundary conditions are retained.

Enforcement of the original three-dimensional continuity equation (28) between adjacent nodes in the vertical (see Figure 1) yields $n-1$ equations:

$$w_i - w_{i-1} = -\int_{z_{i-1}}^{z_i} \nabla \cdot \mathbf{V} \; \mathrm{d}z \quad \text{for } i = 2, \ldots, n. \tag{32}$$

The two boundary conditions (29) and (30) and the $n-1$ equations of (32) constitute a total of $n+1$ equations. The least squares procedure (henceforth 'LS') allows non-zero residuals for the boundary conditions and the conservation of mass equation, much like the data assimilation procedure described by Zahel.[7]

3.4. Adjoint method

A second technique for calculation of vertical velocity developed in the present work is based upon the adjoint approach of Bennett and McIntosh.[8,9] While LS minimizes the residuals of the continuity equation in its discrete form and the two boundary conditions, the adjoint approach ('ADJ') minimizes the residuals of the continuity equation in its continuous form as well as the residuals of the two boundary conditions. The continuity equation and boundary conditions are reconsidered as a variational problem:[10]

$$I = L\int_{-h}^{0} \left(\frac{\partial w}{\partial z} + \nabla \cdot \mathbf{V}\right)^2 \mathrm{d}z + [w - \mathbf{V} \cdot \nabla h]^2_{z=-h} + [w - \mathrm{i}\omega\eta]^2_{z=0}, \tag{33}$$

where L is a scale factor with units of length, introduced for dimensional consistency. Let the function w which minimizes I be called w'. Furthermore, let w_a be an arbitrary function which satisfies the homogeneous boundary conditions $w_\mathrm{a}(-h) = w_\mathrm{a}(0) = 0$. Then the equation

$$w = w' + \epsilon w_\mathrm{a}, \tag{34}$$

where ϵ is an arbitrary constant, represents a one-parameter family of curves that includes the optimal solution w' when $\epsilon = 0$. Every curve in the family satisfies the boundary values of the optimal solution. Furthermore, the optimal solution is assumed to consist of two components:

$$w' = w_\mathrm{t} + w_\mathrm{c}, \tag{35}$$

where w_t is the traditional solution obtained through imposition of just one boundary condition, as described in Section 3.1, and w_c is some correction that will be determined. Insertion of (35) into (34) yields

$$w = w_\mathrm{t} + w_\mathrm{c} + \epsilon w_\mathrm{a}. \tag{36}$$

Substitution of (36) into (33) yields

$$\begin{aligned} I = L\int_{-h}^{0} \left(\frac{\partial(w_\mathrm{t} + w_\mathrm{c} + \epsilon w_\mathrm{a})}{\partial z} + \nabla \cdot \mathbf{V}\right)^2 \mathrm{d}z \\ + [w_\mathrm{t} + w_\mathrm{c} + \epsilon w_\mathrm{a} - \mathbf{V} \cdot \nabla h]^2_{z=-h} + [w_\mathrm{t} + w_\mathrm{c} + \epsilon w_\mathrm{a} - \mathrm{i}\omega\eta]^2_{z=0}. \end{aligned} \tag{37}$$

The optimal correction is the particular correction that minimizes I with respect to ϵ:

$$\begin{aligned} \frac{\partial I}{\partial \epsilon} = 2L\int_{-h}^{0} \frac{\partial w_\mathrm{a}}{\partial z}\left(\frac{\partial(w_\mathrm{t} + w_\mathrm{c} + \epsilon w_\mathrm{a})}{\partial z} + \nabla \cdot \mathbf{V}\right) \mathrm{d}z \\ + 2[w_\mathrm{a}(w_\mathrm{t} + w_\mathrm{c} + \epsilon w_\mathrm{a} - \mathbf{V} \cdot \nabla h)]_{z=-h} + 2[w_\mathrm{a}(w_\mathrm{t} + w_\mathrm{c} + \epsilon w_\mathrm{a} - \mathrm{i}\omega\eta)]_{z=0} = 0. \end{aligned} \tag{38}$$

In addition, it is seen from (34) that the optimal solution is attained when $\epsilon = 0$. For $\epsilon = 0$, (38) becomes

$$0 = L \int_{-h}^{0} \frac{\partial w_a}{\partial z} \left(\frac{\partial (w_t + w_c)}{\partial z} + \nabla \cdot \mathbf{V} \right) \mathrm{d}z + [w_a(w_t + w_c - \mathbf{V} \cdot \nabla h)]_{z=-h} + [w_a(w_t + w_c - \mathrm{i}\omega\eta)]_{z=0}. \tag{39}$$

A residual variable for the continuity equation, λ, is defined as

$$\lambda = \partial(w_t + w_c)/\partial z + \nabla \cdot \mathbf{V}, \tag{40}$$

and (39) becomes

$$0 = L \int_{-h}^{0} \frac{\partial w_a}{\partial z} \lambda \, \mathrm{d}z + [w_a(w_t + w_c - \mathbf{V} \cdot \nabla h)]_{z=-h} + [w_a(w_t + w_c - \mathrm{i}\omega\eta)]_{z=0}. \tag{41}$$

Integration by parts of the first term to shift derivatives from w_a to λ yields

$$0 = -L \int_{-h}^{0} \frac{\partial \lambda}{\partial z} w_a \, \mathrm{d}z + [w_a(w_t + w_c - \mathbf{V} \cdot \nabla h - L\lambda)]_{z=-h} + [w_a(L\lambda + w_t + w_c - \mathrm{i}\omega\eta)]_{z=0}. \tag{42}$$

Because w_a is arbitrary, satisfaction of (42) requires three conditions:

(i) $\partial\lambda/\partial z = 0$,

(ii) $[w_t + w_c - \mathbf{V} \cdot \nabla h - L\lambda]_{z=-h} = 0$,

(iii) $[L\lambda + w_t + w_c - \mathrm{i}\omega\eta]_{z=0} = 0$.

Furthermore, it is assumed that w_t is obtained by imposition of the bottom boundary condition, with the surface boundary condition neglected, such that in general

$$\partial w_t/\partial z = -\nabla \cdot \mathbf{V}, \tag{43}$$

$$[w_t = \mathbf{V} \cdot \nabla h]_{z=-h}, \tag{44}$$

$$[w_t \neq \mathrm{i}\omega\eta]_{z=0}. \tag{45}$$

Integration of condition (i) yields

$$\lambda = c_1, \tag{46}$$

where c_1 is a constant of integration. Insertion of definition (40) of λ yields

$$\partial(w_t + w_c)/\partial z + \nabla \cdot \mathbf{V} = c_1. \tag{47}$$

However, w_t has been assumed to exactly satisfy the governing equation as stated in (43), so (47) reduces to

$$\partial w_c/\partial z = c_1. \tag{48}$$

Integration of (48) yields

$$w_c = c_1 z + c_2, \tag{49}$$

where c_2 is another constant of integration.

Determination of the integration constants in (49) requires two boundary conditions, one of which may be attained from condition (ii):

$$[w_t + w_c - \mathbf{V} \cdot \nabla h - L\lambda]_{z=-h} = 0. \tag{50}$$

Since w_t has been assumed to exactly satisfy the bottom boundary condition, (50) reduces to

$$[w_c - L\lambda]_{z=-h} = 0. \tag{51}$$

In addition, $\lambda = c_1$ from (46), so (51) yields one of the required boundary conditions for (49):

$$w_c|_{z=-h} = Lc_1. \tag{52}$$

The constant of integration c_2 can now be determined from (49) as

$$c_2 = c_1(L + h) \tag{53}$$

and insertion of (53) into expression (49) yields for the correction

$$w_c = c_1(L + h + z). \tag{54}$$

The second required boundary condition may be obtained from condition (iii):

$$[L\lambda + w_t + w_c - i\omega\eta]_{z=0} = 0. \tag{55}$$

Substitution of (54) into (55) yields an expression for c_1:

$$c_1 = \frac{i\omega\eta - w_t|_{z=0}}{2L + h}. \tag{56}$$

Substitution of (56) into (54) yields the desired correction

$$w_c = \left(\frac{i\omega\eta - w_t|_{z=0}}{2L + h}\right)(L + h + z), \tag{57}$$

which is a linear function of the misfit between the traditional solution at the surface and the neglected surface boundary condition.

If the traditional solution is obtained with the surface boundary condition and the adjoint procedure is repeated, a different correction term is obtained:

$$w_c = \left(\frac{w_t - \mathbf{V} \cdot \nabla h|_{z=-h}}{2L + h}\right)(z - L). \tag{58}$$

Regardless of which boundary condition is used in the determination of w_t, the same optimal solution is obtained when the appropriate correction w_c is applied.

4. QUARTER-ANNULAR HARBOUR

A particularly attractive departure point for comparison of the behaviour of TRAD, VDC, LS and ADJ is a study of an annular harbour, because an analytic solution for the vertical velocity is known. The analytic solution for the depth-averaged case was developed by Lynch and Gray[11] for constant, linear and quadratic bathymetry for both steady state wind set-up and periodic tidal response. This analytic solution has been used extensively as a test case for two-dimensional finite element shallow water codes.[12–14] The analytic solution was extended to three dimensions by Lynch and Officer[15] for tidal oscillations near a circular island where the tidal amplitude at the open ocean boundary varies with position. For the purposes of this study the analytic solution of Lynch and Officer[15] is considered with spatially constant tidal amplitude forcing at the open ocean boundary.

4.1. Description of quarter-annular harbour problem

The geometry of the quarter-annular harbour is shown in Figure 2(a). The boundaries at $r = r_1 = 4 \times 10^4$ m, $\theta = 0$ and $\theta = \pi/2$ are no-flow boundaries. The open boundary, located at

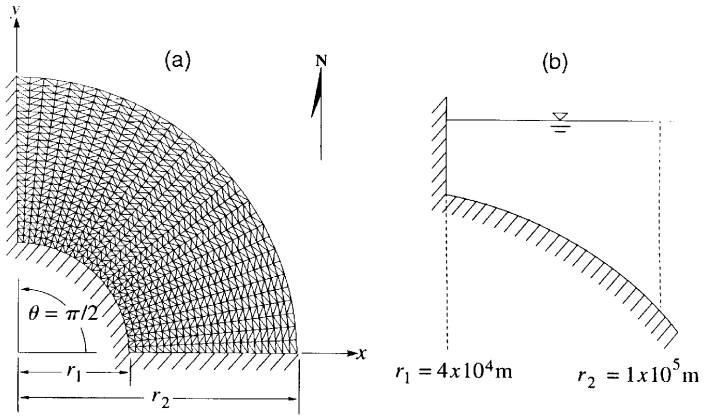

Figure 2. (a) Section view of quarter-annular harbour with opening at $r = r_2$. (b) Side view of quarter-annular harbour with quadratic bottom

$r = r_2 = 1 \times 10^5$ m, is forced by an M_2 tide with frequency $1{\cdot}405 \times 10^{-4}\,s^{-1}$ and amplitude 0·1 m. The horizontal grid, as shown in Figure 2(a), was generated with XMGREDIT, a flexible interactive grid generation code developed by Turner and Baptista.[16] The bottom of the harbour, as shown in Figure 2(b), is quadratic in r and constant in θ such that $h = r^2/H$, with $H = 1{\cdot}6 \times 10^8$ m. The grid contains 825 nodes and 1536 elements. The analytic solution with constant amplitude forcing, including the vertical velocity, which is not determined by Lynch and Officer,[15] is found in the Appendix.

4.2. *Behaviour of three methods of calculation of vertical velocity*

The vertical velocities are computed using four methods: the traditional method (TRAD), the vertical derivative of the continuity method (VDC), the least squares method (LS) and the adjoint method (ADJ) with $L = 1$ m. All solutions presented are converged; further refinement of the horizontal and vertical grids does not significantly change the solution.

Two typical vertical velocity profiles are shown in Figures 3 and 4. The analytic vertical velocity profile is computed with the analytic horizontal velocity profile, while the four approximate vertical velocity profiles are computed with the horizontal velocity profiles obtained from the finite element solution. However, the analytic and finite element horizontal profiles are nearly identical. The vertical velocity profiles shown in these figures are representative of profiles obtained throughout the tidal cycle for various values of K, λ and r. The profiles in Figure 3 are obtained at one-eighth of the tidal cycle with $r = 82{,}500$ m, $\lambda = 9{\cdot}206 + 9{\cdot}206$i and $K = 2{\cdot}836$, while the profiles in Figure 4 are obtained at the beginning of the tidal cycle with $r = 70{,}000$ m, $\lambda = 6{\cdot}627 + 6{\cdot}627$i and $K = 102{\cdot}1$. Although these solutions are converged, TRAD, LS and ADJ converge to a different solution from VDC. Most importantly, the TRAD, LS and ADJ solutions are nearly identical with the analytic solution. In fact, for all profiles studied, the TRAD, LS and ADJ solutions more closely approximate the analytic solution than does VDC.

4.3. *Conservation of mass analysis*

It has been shown that, at least for the quarter-annular harbour test case, TRAD, LS and ADJ approximate the analytic vertical profile more accurately than VDC. However, an analytical solution will not be available for natural domains. A conservation of mass analysis is undertaken to establish a

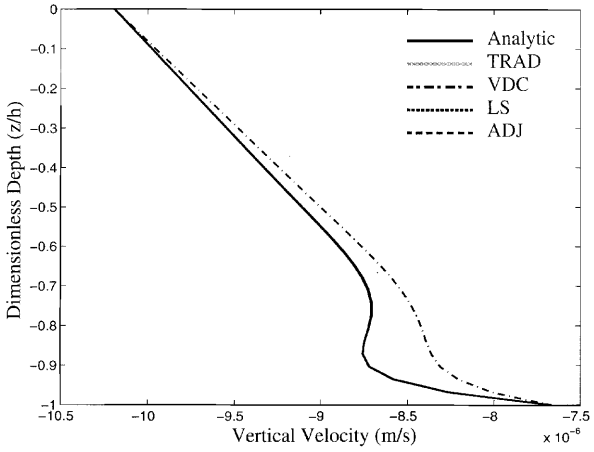

Figure 3. Vertical velocity profile calculated with TRAD, VDC, LS and ADJ compared with analytic solution at one-eighth of a tidal cycle, with $r = 82{,}500$ m, $\lambda = 9{\cdot}206 + 9{\cdot}206\mathrm{i}$ and $K = 2{\cdot}836$

criterion for comparison of the three methods that does not rely upon the availability of an analytic solution.

For an incompressible fluid the expression of the principle of conservation of mass for a fixed volume with outer surface Γ is

$$\int_{\Gamma} (\mathbf{V} + w\hat{\mathbf{z}}) \cdot \hat{\mathbf{n}} \, d\Gamma = 0, \tag{59}$$

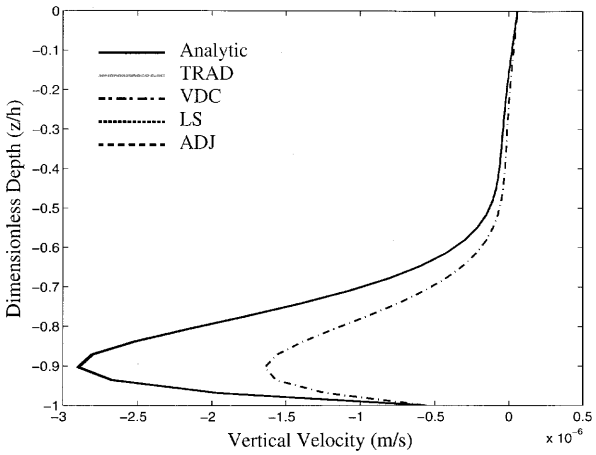

Figure 4. Vertical velocity profile calculated with TRAD, VDC, LS and ADJ compared with analytic solution at beginning of a tidal cycle, with $r = 70{,}000$ m, $\lambda = 6{\cdot}627 + 6{\cdot}627\mathrm{i}$ and $K = 102{\cdot}1$

where $\hat{\mathbf{n}}$ is the outward normal vector to the surface Γ and $\hat{\mathbf{z}}$ is the unit vector in the vertical direction. In the case of an approximate solution, (59) takes the form

$$\int_{\Gamma} (\mathbf{V} + w\hat{\mathbf{z}}) \cdot \hat{\mathbf{n}} \, d\Gamma = Res, \tag{60}$$

where *Res* is a residual. The residual is examined using TRAD, VDC, LS and ADJ with the surface of one three-dimensional finite element serving as the surface of integration in equation (60). The vertical faces and the top and bottom surfaces of the element will be considered separately:

$$Res = \sum_{k=1}^{3} \left(\int_{\Gamma_{v,k}} (\mathbf{V} + w\hat{\mathbf{z}}) \cdot \hat{\mathbf{n}} \, d\Gamma_{v,k} \right) + \int_{\Gamma_t} (\mathbf{V} + w\hat{\mathbf{z}}) \cdot \hat{\mathbf{n}} \, d\Gamma_t + \int_{\Gamma_b} (\mathbf{V} + w\hat{\mathbf{z}}) \cdot \hat{\mathbf{n}} \, d\Gamma_b, \tag{61}$$

where $\Gamma_{v,k}$, $k = 1, 2, 3$, are the three vertical faces and Γ_t and Γ_b are the top and bottom surfaces respectively.

As an example, the residual is computed over several tidal cycles for the single element centred at $r = 70{,}800$ m and $\sigma = -0{\cdot}322$ ($z = -13{\cdot}7$ m). The residual versus time is plotted in Figure 5. The residual obtained by all three methods is a sinusoidal wave with a period of 12·42 h, the same period as the forcing. However, the amplitude of the residual obtained with VDC is $0{\cdot}74\,m^3\,s^{-1}$, while the residual obtained with TRAD, LS and ADJ has an amplitude of $0{\cdot}015\,m^3\,s^{-1}$, less by a factor of 50. This behaviour is typical for elements throughout the three-dimensional domain. Although the traditional method conserves mass exactly over each one-dimensional vertical system, mass conservation will not be exact in a three-dimensional element unless the velocity variation between nodes is linear.

5. SOUTHWESTERN VANCOUVER ISLAND

This section examines vertical velocity calculations in the portion of the Pacific Ocean adjacent to the southwestern coast of Vancouver Island, as shown in Figure 6. The region is bounded by Vancouver

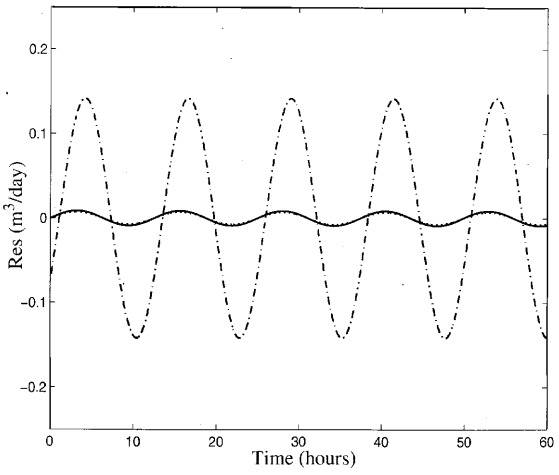

Figure 5. Residual versus time calculated with TRAD, VDC, LS and ADJ at $r = 70{,}800$ m and $\sigma = -0{\cdot}322$. See Figures 3 or 4 for key to curves

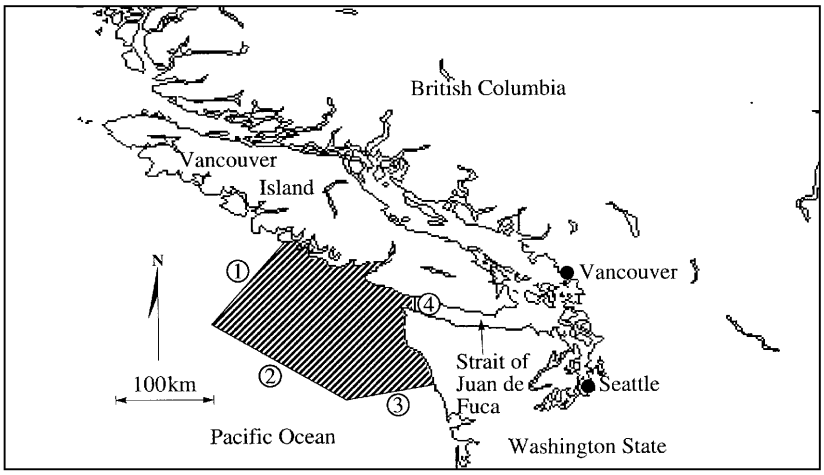

Figure 6. Map of southwestern Vancouver Island area

Island on the northeast and Washington State on the east. Open ocean boundaries 1, 2 and 3 lie in the Pacific Ocean and boundary 4 lies at the opening of the Strait of Juan de Fuca.

The bottom topography of the region is shown in Figure 7. The region is characterized by an extensive continental shelf, a steep continental slope and a broad continental rise.[17] The Juan de Fuca Canyon, which is about 10 km wide and 400 m deep, runs roughly north/south through the eastern portion of the domain. Jutting northward from the Juan de Fuca Canyon is a second, smaller canyon known as the Spur[18] or Tully[19] Caynon. The Tully Canyon is associated with a summer upwelling event known as the Tully Eddy which causes a near-surface mass of high-density water. The eddy affects temperature, salinity, nutrients and dissolved oxygen fields and is likely a major source of nutrients for the southern Vancouver Island shelf.[18] A better understanding and more accurate

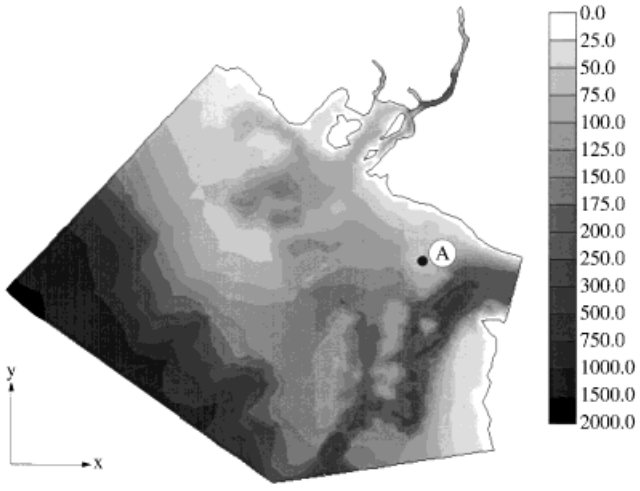

Figure 7. Bathymetry of southwestern Vancouver Island domain

prediction of vertical velocities in this region would be very useful to fishery scientists and management.

5.1. Forcing

To study the performance of TRAD, VDC, LS and ADJ in a complex domain while maintaining a certain amount of control over the response of the system, the system is forced with a steady wind, attained by setting $h\boldsymbol{\Psi} = (-0{\cdot}001, 0{\cdot}001)\,\mathrm{m^2\,s^{-2}}$ in the surface boundary condition (4). This stress value corresponds to a wind of magnitude $7\,\mathrm{m\,s^{-1}}$ from the southeast, a typical winter wind. Figure 8, which shows the surface currents attained with this forcing, provides an indication of the response of the system.

5.2. Boundary conditions

No-normal-flow boundary conditions are imposed at all land boundaries. To prevent wetting and drying of elements, the minimum bathymetric depth is set to 10 m. Boundary 1 is treated as a geostrophic boundary such that the elevation gradient and transport are in geostrophic balance,[5] while boundaries 2, 3 and 4 are specified as having zero elevation.

5.3. Convergence study

Interval halving is used to determine the convergence of this numerical problem. The domain is discretized with three grids as follows. The first grid, SWVI1, is a coarse grid consisting of 1396 nodes and 2519 elements, as shown in Figure 9. It is derived from the more extensive grid of Foreman *et al.*[20] that covers the entire west coast of Vancouver Island. The grid is designed to compromise among three design requirements; (i) a close fit of the grid to the coastline, (ii) a near-equilateral element shape and (iii) a near-uniform ratio of element area to bathymetric depth.[21] These three criteria are similar to those developed by Westerink *et al.*[22,23] The second grid, SWVI2, is created by dividing each element in SWVI1 into four elements, as illustrated in Figure 10. SWVI2 contains 5390 nodes and 10,216 elements. The same refinement procedure is repeated to create a third grid, SWVI3,

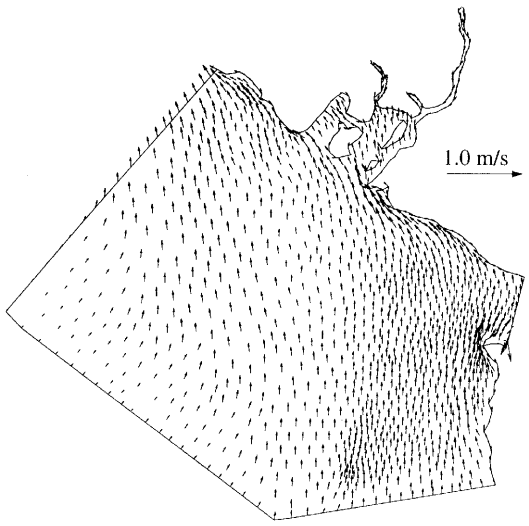

Figure 8. Surface currents resulting from steady $7\,\mathrm{m\,s^{-1}}$ wind from southeast

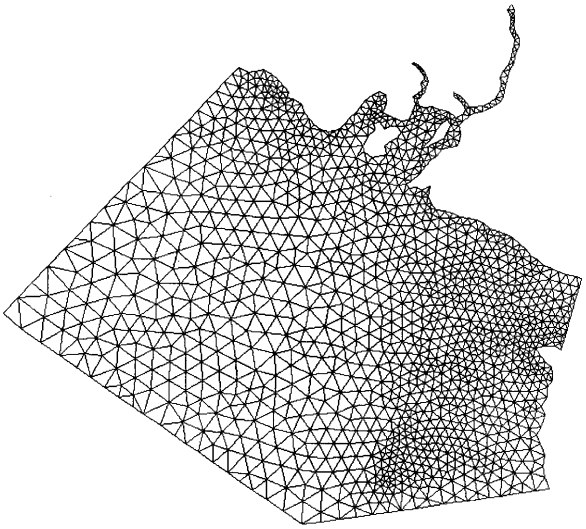

Figure 9. Coarse grid of southwestern Vancouver Island

consisting of 20,988 nodes and 40,864 elements. The bathymetry fields of all three grids are identical; the nodal values for the bathymetry in SWVI2 and SWVI3 are obtained through linear interpolation of the bathymetry in SWVI1. The results presented here are produced with 15 σ-layers in the vertical. The bottom friction and vertical eddy viscosity values used in this example are $0{\cdot}015\,\mathrm{m\,s^{-1}}$ and $0{\cdot}01\,\mathrm{m^2\,s^{-1}}$ respectively. All solutions presented are converged in the vertical; additional layers do not substantially affect the solution.

Figure 11 shows the vertical profiles of the lateral velocities for node A, whose location on Swiftsure Bank is indicated in Figure 7. These horizontal profiles are converging well; the difference between the solutions obtained with SWVI2 and SWVI3 is roughly one-third of the difference between the solutions obtained with SWVI1 and SWVI2. Although the profiles differ quantitatively throughout the domain, the convergence behaviour of this node is representative of the entire domain.

Next the vertical velocity profiles at node A obtained with TRAD, VDC, LS and ADJ are shown in Figure 12. These vertical profiles are representative of the qualitative behaviour of the profiles obtained throughout the domain, although the profiles differ quantitatively. Three important features are illustrated by this figure. First, the scales of parts (a), (b) and (c) are identical; the differences in the profiles are significant. The vertical velocity solution shows disagreement in both magnitude and direction of the flow. VDC predicts downwelling in the bottom portion of the domain, while TRAD, LS and ADJ predict upwelling. Secondly, the solutions obtained with LS and ADJ are nearly identical, but differ markedly from the TRAD solution, especially with coarse resolution and at the

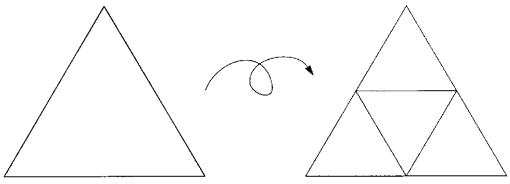

Figure 10. Grid refinement procedure

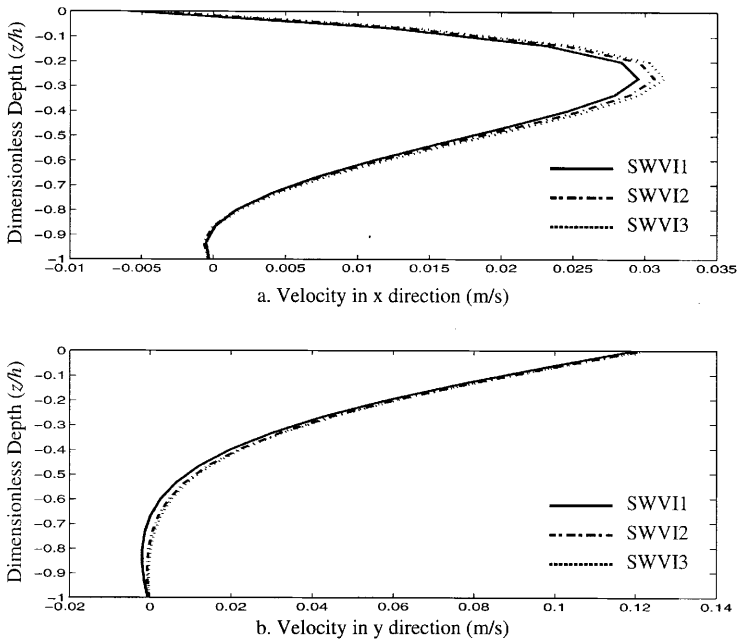

Figure 11. Horizontal velocity profiles at node A in Figure 7

surface. Finally, in all three cases the vertical velocity is dependent upon the resolution of the horizontal grid and is therefore sensitive to the degree of convergence of the horizontal velocity solution.

5.4. *Conservation of mass*

It has been shown that the computed vertical velocity profile is dependent on the computation method in the southwest Vancouver Island domain. The conservation of mass properties of the four methods are considered here in an effort to make a definitive statement as to which method leads to a more realistic vertical velocity profile.

The residual for each element of the three-dimensional conservation of mass equation is computed as described in Section 4.3 and summed over each σ-layer:

$$Res_j^* = \sum_i^{\text{elements}} Res_{ij} \quad \text{for } j = 1, \ldots, n_\sigma - 1, \tag{62}$$

where i represents the horizontal element number, j represents the vertical σ-layer and n_σ is the number of nodes in the vertical. The summation leads to a total residual Res_j^* for each σ-layer j. Figure 13 is a plot of dimensionless depth versus the corresponding Res_j^* for TRAD, VDC, LS and ADJ. The VDC residual has large deviations from zero at the surface and at the bottom where the boundary conditions are enforced exactly.

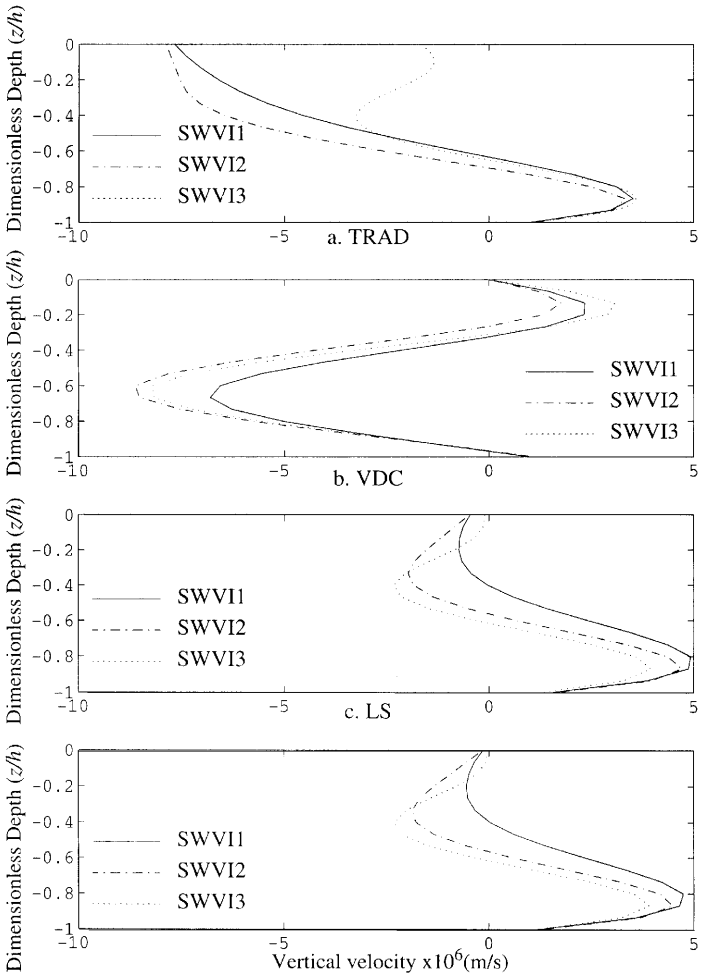

Figure 12. Vertical velocity profiles at node A in Figure 7

The Res_j^* calculation described in (62) allows error cancellation between positive and negative residuals within each layer. To examine the extent of error cancellation, the layer residual calculation is repeated with the absolute value of the residual,

$$Res_j^{*\mathrm{abs}} = \sum_{i}^{\text{elements}} |Res_{ij}|, \tag{63}$$

and the results are shown in Figure 14. Throughout the profile the $Res_j^{*\mathrm{abs}}$ obtained with TRAD, LS and ADJ is much closer to zero than that obtained with VDC. While the VDC residual diverges from zero with increasing horizontal resolution (Figure 14(b)), the TRAD, LS and ADJ residual converges towards zero as the horizontal resolution increases (Figures 14(a), 14(c) and 14(d)).

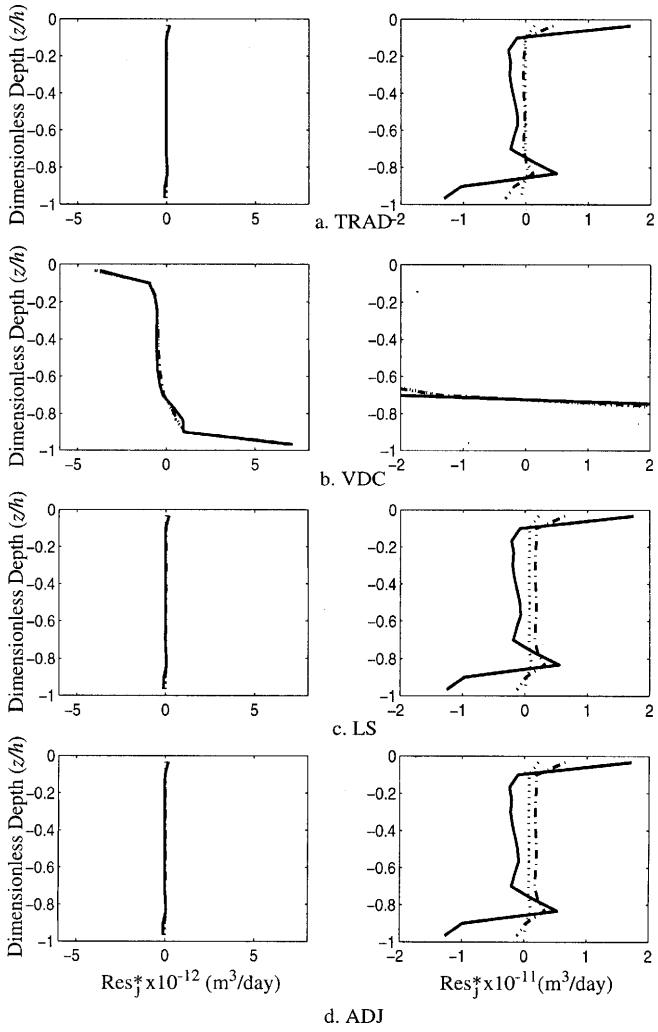

Figure 13. Residual profiles obtained with TRAD, VDC, LS and ADJ (full view on left, close-up view on right) for SWVI1 (——), SWVI2 (- - -) and SWVI3 (. . . . . .)

6. CONCLUSIONS

Two methods of vertical velocity calculations that assimilate additional information at the boundary (previously LS and ADJ) are proposed and examined within the confines of the three-dimensional finite element model. The performance of these methods is compared with both a traditional approach which neglects some of the boundary information (previously TRAD) and an approach which solves the vertical derivative of the continuity equation with two boundary conditions (previously VDC). In a quarter-annular harbour domain, the TRAD, LS and ADJ better approximate the analytic solution and have better mass conservation properties than VDC. Furthermore, the former three approaches have almost identical behaviour. An application to the southwestern Vancouver Island domain shows

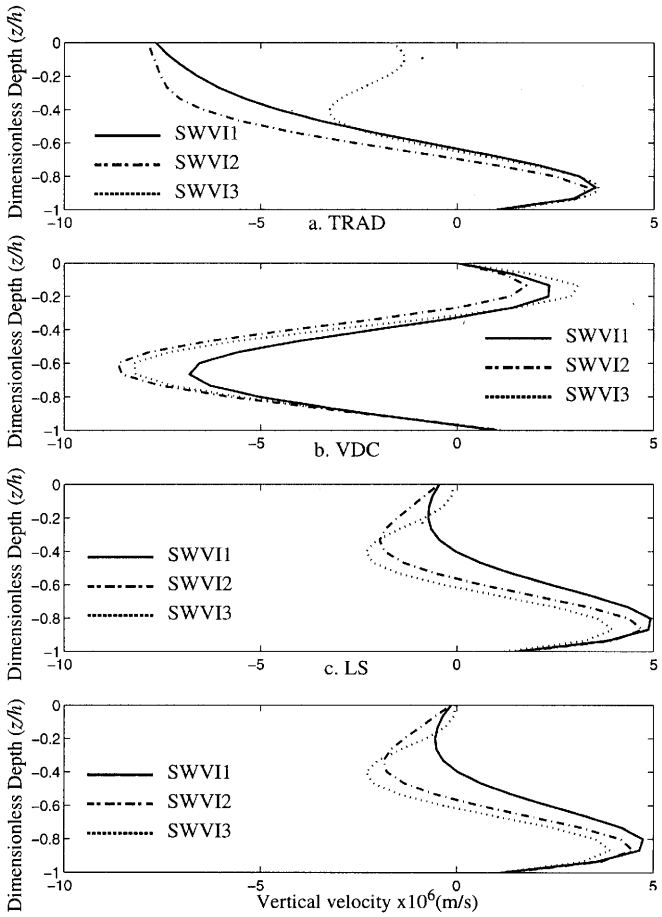

Figure 14. Absolute residual profiles obtained with TRAD, VDC, LS and ADJ

that the vertical velocity profile is dramatically dependent upon the method of calculation. In this domain the vertical velocity obtained with TRAD shows a large deviation from the neglected boundary condition. As with the quarter-annular harbour, TRAD, LS and ADJ have better mass conservation properties than VDC. Furthermore, the deterioration in mass conservation which arises from allowing residuals in the conservation of mass equation (in both LS and ADJ) is quite small.

The vertical velocity profiles and hence the mass conservation properties obtained with LS and ADJ are nearly identical throughout this analysis. These methods clearly outperform VDC in both the quarter-annular harbour and the southwestern Vancouver Island studies. Although TRAD, LS and ADJ demonstrate nearly equivalent results in the quarter-annular harbour study, in the southwestern Vancouver Island study the TRAD method clearly does not satisfy the neglected boundary condition, while LS and ADJ account for this condition. The least squares method has larger CPU and memory requirements as it requires a matrix multiplication and then solution of a system of linear algebraic equations. Implementation of the adjoint method is very simple as it involves only a traditional

calculation of the vertical velocity and then an algebraic calculation for a correction. It is therefore concluded that the optimal method for computation of vertical velocity in a three-dimensional finite element model is the adjoint method.

ACKNOWLEDGEMENTS

This research has been funded by a National Science Foundation Graduate Research Fellowship and Rice University subcontract of NSF funding R34111-77600094. The authors would also like to thank Paul Hamblin for his helpful suggestions.

APPENDIX: ANALYTIC SOLUTION WITH CONSTANT AMPLITUDE FORCING

A radial co-ordinate system is used for the analytical solution to the quarter-annular test problem. Because the governing equations, boundary conditions and domain geometry do not depend on θ, variation occurs only in the radial and vertical directions.

The equations to be solved are the linearized horizontal momentum equation in periodic form, with Coriolis force neglected,

$$\mathrm{i}\omega V_{\mathrm{R}} + g\nabla\eta - \frac{\partial}{\partial z}\left(N\frac{\partial V_{\mathrm{R}}}{\partial z}\right) = 0, \tag{64}$$

and the linearized, depth-averaged continuity equation in periodic form,

$$\mathrm{i}\omega\eta + \nabla\cdot(h\bar{V}_{\mathrm{R}}) = 0, \tag{65}$$

where $V_{\mathrm{R}}(r,z)$ is the component of the velocity in the radial direction, $\bar{V}_{\mathrm{R}}(r)$ is the vertical average of V_{R}, $\eta(r)$ is a function only of r, N is constant, ∇ is the horizontal del operator in radial co-ordinates and (r,z) are the radial and vertical co-ordinates respectively.

In the horizontal the no-normal-flow boundary condition is enforced on the land boundaries, i.e.

$$\partial\eta/\partial r = 0 \quad \text{at } r = r_1, \qquad \partial\eta/\partial\theta = 0 \quad \text{at } \theta = 0, \pi/2,$$

and the elevation is specified on the open boundary, i.e.

$$\eta = \mathrm{Re}\{\eta_0 \mathrm{e}^{\mathrm{i}\omega t}\} \quad \text{at } r = r_2.$$

A stress boundary condition is enforced at the surface as described by (2), but with no wind stress. In addition, since it has been shown that bottom stress may be expressed in terms of vertically averaged velocity with a complex slip coefficient, the bottom boundary condition is restated as

$$N\frac{\partial V_{\mathrm{R}}}{\partial z}\bigg|_{z=-h} = \tau h\bar{V}_{\mathrm{R}}, \tag{66}$$

where τ is an unknown complex, linear slip coefficient to be determined later.

Surface elevation

The vertical average of (64), after incorporation of boundary conditions (2) and (66), is

$$(\mathrm{i}\omega + \tau)\bar{V}_{\mathrm{R}} + g\nabla\eta = 0. \tag{67}$$

$\bar{V}_R$ can be eliminated among (65) and (67) to obtain a wave equation in η alone:

$$i\omega\eta - \nabla \cdot \left(\frac{gh}{i\omega + \tau} \nabla\eta \right) = 0. \tag{68}$$

The surface elevation η can now be calculated from (68) and appropriate boundary conditions. Lynch and Gray[11] implement separation of variables to determine the solution to (68):

$$\eta(r, t) = \mathrm{Re}\{(Ar^{s_1} + Br^{s_2})e^{i\omega t}\}, \tag{69}$$

where

$$A = \frac{\eta_0 s_2 r_1^{s_2}}{s_2 r_2^{s_1} r_1^{s_2} - s_1 r_1^{s_1} r_2^{s_2}}, \qquad B = \frac{-\eta_0 s_1 r_1^{s_1}}{s_2 r_2^{s_1} r_1^{s_2} - s_1 r_1^{s_1} r_2^{s_2}},$$
$$s_1 = -1 + \sqrt{(1 - \beta^2)}, \qquad s_2 = -1 - \sqrt{(1 - \beta^2)}, \qquad \beta^2 = (\omega^2 - i\omega\tau)/(gh_0).$$

An expression for τ is yet to be determined.

Horizontal velocity field

The horizontal velocity field will be obtained from the momentum equation (64) and the surface elevation field (69). The vertical co-ordinate of the momentum equation will be stretched to a σ-co-ordinate system such that $\sigma = z/h$. Accordingly, the moment equation (64) may be rewritten as

$$V_R - \frac{\partial}{\partial\sigma} \left(\frac{N}{i\omega h^2} \frac{\partial V_R}{\partial\sigma} \right) = V_{0R}, \tag{70}$$

where

$$V_{0R} = -g \frac{\nabla\eta}{i\omega}. \tag{71}$$

Incorporation of the elevation solution (69) in (71) yields

$$V_{0R} = -\frac{g}{i\omega r} (s_1 A r^{s_1} + s_2 B r^{s_2}) e^{i\omega t}. \tag{72}$$

A particular solution to (70) is $V_R = V_{0R}$, so the general solution is

$$V_R = V_{0R} + C_1\mu_1(\sigma) + C_2\mu_2(\sigma), \tag{73}$$

where μ_1 and μ_2 are scalar functions that satisfy the homogeneous form of (70):

$$\mu_1 = \exp(\sigma\lambda), \qquad \mu_2 = \exp(-\sigma\lambda),$$

with $\lambda = \sqrt{(i\omega h^2/N)}$. The constants of integration C_1 and C_2 are determined by requiring (73) to satisfy the boundary conditions (2) and (66). The horizontal velocity field is

$$V_R = V_{0R} \left(1 - \frac{\cosh(\lambda\sigma)}{\cosh\lambda[1 + (\lambda/K)\tanh\lambda]} \right), \tag{74}$$

where $K = kh/N$ is the dimensionless slip coefficient. The vertical average of $\mathbf{V}$ is obtained through integration of (74) over the depth:

$$\bar{V}_R = V_{0R} \left(1 - \frac{\tanh\lambda}{\lambda[1 + (\lambda/K)\tanh\lambda]} \right). \tag{75}$$

Complex bottom slip coefficient

Once V_R and $\bar{V}_R$ are known, τ can be determined from the bottom boundary condition (66), in σ-co-ordinates, as

$$\frac{N}{h}\frac{\partial V_R}{\partial \sigma}\bigg|_{\sigma=-1} = \tau h \bar{V}_R. \tag{76}$$

After substitution of (74) and (75), some algebraic manipulation yields an expression for τ:

$$\tau = \frac{N}{h^2}\left(\frac{\lambda^2 \tanh\lambda}{\lambda + (\lambda^2/K - 1)\tanh\lambda}\right). \tag{77}$$

This relationship between known parameters K, λ and N and the complex bottom stress coefficient completes the surface elevation solution (69) and the horizontal velocity solution (74). For the remainder of the derivation, τ will be constant, i.e. N and k vary with h such that λ and K remain constant.

Vertical velocity

To obtain the complete three-dimensional velocity field, the vertical velocity must be determined from the continuity equation. In three dimensions and radial co-ordinates, with variation in the θ-direction neglected, the continuity equation is

$$\frac{1}{r}\frac{\partial}{\partial r}(rV_R) + \frac{\partial w}{\partial z} = 0. \tag{78}$$

Transformation into σ-co-ordinates ($\sigma = z/h, r = R$), use of the bathymetry relationship $h = r^2/H$ and implementation of the chain rule to evaluate the derivatives yields

$$\frac{\partial}{\partial r} = \frac{\partial \sigma}{\partial r}\frac{\partial}{\partial \sigma} + \frac{\partial R}{\partial r}\frac{\partial}{\partial R} = -\frac{2\sigma}{r}\frac{\partial}{\partial \sigma} + \frac{\partial}{\partial R},$$

$$\frac{\partial}{\partial z} = \frac{\partial \sigma}{\partial z}\frac{\partial}{\partial \sigma} + \frac{\partial R}{\partial z}\frac{\partial}{\partial R} = \frac{H}{r^2}\frac{\partial}{\partial \sigma}.$$

Equation (78) may be written as

$$-\frac{2\sigma}{H}\frac{\partial}{\partial \sigma}(RV_R) + \frac{r}{H}\frac{\partial}{\partial R}(RV_R) + \frac{\partial w}{\partial \sigma} = 0. \tag{79}$$

Integration of (79) over σ and incorporation of the bottom boundary condition $w|_{\sigma=-1} = -2V_R R/H$ yields

$$w(\sigma) = \frac{2}{H}\int_{-1}^{\sigma} \sigma \frac{\partial}{\partial \sigma}(RV_R)\, \mathrm{d}\sigma - \frac{r}{H}\int_{-1}^{\sigma} \frac{\partial}{\partial R}(RV_R) d\sigma - \frac{2V_R R}{H}. \tag{80}$$

Evaluation of the derivatives and appropriate integration yields the analytic vertical velocity solution

$$w(\sigma) = 2\gamma\alpha_1\delta\left(\frac{\sigma\cosh(\lambda\sigma) + \cosh\lambda}{\lambda} - \frac{\sinh(\lambda\sigma) + \sinh\lambda}{\lambda^2}\right)$$
$$+ \gamma\alpha_2\left(\sigma + 1\,\frac{\delta\sinh(\lambda\sigma) + \sinh\lambda}{\lambda^2}\right) + 2\gamma\alpha_1\left(1 - \frac{\delta\cosh\lambda}{\lambda}\right),$$

where

$$\gamma = \frac{gh_0}{\mathrm{i}\omega}\exp(\mathrm{i}\omega t), \qquad \delta = \frac{\lambda}{\cosh\lambda[1 + (\lambda/K)\tanh\lambda]},$$
$$\alpha_1 = As_1R^{s_1} + Bs_2R^{s_2}, \qquad \alpha_2 = As_1^2R^{s_1} + Bs_2^2R^{s_2}.$$

REFERENCES

1. D. R. Lynch and W. G. Gray, 'A wave equation model for finite element computations', *Comput. Fluids*, **2**, 135–153 (1979).
2. D. R. Lynch and F. E. Werner, 'Three-dimensional hydrodynamics on finite elements. Part 1: Linearized harmonic model', *Int. j. numer. methods fluids*, **7**, 871–909 (1987).
3. R. A. Luettich, J. J. Westerink and N. W. Scheffner, 'ADCIRC: an advanced three-dimensional circulation model for shelves, coasts and estuaries, Report 1: Theory and methodology of ADIRC-2DDI and ADCIRC-3DL', *Tech. Rep. DRP-92-6*, Department of the Army, Washington, DC, 1991.
4. D. R. Lynch, F. E. Werner, D. A. Greenberg and J. W. Loder, 'Diagnostic model for baroclinic, wind-driven and tidal circulation in shallow seas', *Continental Shelf Res.*, **12**, 36–64 (1992).
5. C. E. Naimie and D. R. Lynch, 'Three-dimensional diagnostic model for baroclinic, wind-driven and tidal circulation in shallow seas', *FUNDY5 User's Manual*, Dartmouth College, 1993.
6. G. H. Golub and C. F. Van Loan, *Matrix Computations*, Johns Hopkins University Press, Baltimore, MD, 1983.
7. W. Zahel, 'Modelling ocean tides with and without assimilating data', *J. Geophys. Res.*, **96**(B12), 20,379–20,391 (1991).
8. A. F. Bennett and P. C. McIntosh, 'Open ocean modeling as an inverse problem: tidal theory', *J. Phys. Oceanogr.*, **12**, 1004–1018 (1982).
9. P. C. McIntosh and A. F. Bennett, 'Open ocean modeling as an inverse problem: M_2 tides in Bass Strait', *J. Phys. Oceanogr.*, **14**, 601–614 (1984).
10. G. A. Bliss, *Calculus of Variations*, Open Court, LaSalle, IL, 1925.
11. D. R. Lynch and W. G. Gray, 'Analytic solutions for computer flow model testing', *J. Hydraul. Div., ASCE*, **104**(HY10), 1409–1428 (1978).
12. W. G. Gray and D. R. Lynch, 'On the control of noise in finite element tidal computations: a semi-implicit approach', *Comput. Fluids*, **7**, 47–67 (1978).
13. W. G. Gray, 'Some inadequacies of finite element models is simulators of two-dimensional circulation', *Adv. Water Rescources*, **5**, 171–177 (1982).
14. J. J. Westerink, R. A. Luettich, J. K. Wu and R. L. Kolar, 'The influence of normal flow boundary conditions on spurious modes in finite element solutions to the shallow water equations', *Int. j. numer. methods fluids*, **18**, 1021–1060 (1994).
15. D. R. Lynch and C. B. Officer, 'Analytic test cases for three-dimensional hydrodynamic models', *Int. j. numer. methods fluids*, **5**, 529–543 (1985).
16. P. J. Turner and A. M. Baptista, 'ACE/Gredit user's manual: software for semi-automatic generation of two-dimensional finite element grids', *CCALMR Software Rep. SDS2(91-2)*, Oregon Graduate Institute, Beaverton, OR, 1991.
17. R. A. Walters and M. G. G. Foreman, 'A 3D, finite element model for baroclinic circulation on the Vancouver Island continental shelf', *J. Marine Syst.*, **3**, 5070–518 (1992).
18. J. J. Freeland and K. L. Denman, 'A topographically controlled upwelling center off southern Vancouver Island', *J. Marine Res.*, **40**, 1069–1093 (1982).
19. H. Freeland and P. McIntosh, 'The vorticity balance on the southern British Columbia continential shelf', *Atmosphere–Ocean*, **27**, 643–657 (1989).
20. M. G. G. Foreman, R. E. Thomson, D. R. Lynch and R. A. Walters, 'A finite element model for three-dimensional flows along the west coast of Vancouver Island', *Proc. 2nd Int. Conf. on Estuarine and Coastal Modelling*, ASCE, New York, 1992, pp. 574–585.
21. M. G. G. Foreman and R. A. Walters, 'A finite element tidal model for the southwest coast of Vancouver Island', *Atmosphere–Ocean*, **28**, 261–287 (1989).
22. J. J. Westerink, J. C. Muccino and R. A. Luettich, 'Resolution requirements for a tidal model of the western North Atlantic and Gulf of Mexico', in *Computational Methods in Water Resources IX*, Vol. 2, *Mathematical Modeling in Water Resources*, Computational Mechanics Publications, Southampton, 1992, pp. 637–648.
23. J. J. Westerink, R. A. Luettich and J. C. Muccino, 'Modeling tides in the western North Atlantic using unstructured graded grids', *Tellus*, **46A**, 178–199 (1994).

